An Anisotropic BRDF Model for Fitting and Monte Carlo Rendering

Murat Kurt*
International Computer Institute
Ege University

László Szirmay-Kalos†
TU Budapest

Jaroslav Křivánek‡
Cornell University
Charles University in Prague

Abstract

In this paper we propose a new physically plausible, anisotropic Bidirectional Reflectance Distribution Function (BRDF) for fitting and for importance sampling in global illumination rendering. We demonstrate that the new model is better in data fitting than existing BRDF models. We also describe efficient schemes for sampling the proposed anisotropic BRDF model. Furthermore, we test it on a GPU-based real-time rendering algorithm and show that material design can be done with this anisotropic BRDF model effectively. We also show that the new model has effective real-time rendering performance.

CR Categories: I.3.7 [Computer Graphics]: Three-Dimensional Graphics and Realism—Color, shading, shadowing, and texture

Keywords: anisotropic, BRDF, global illumination

1 Introduction

Global illumination algorithms solve the rendering equation [Kajiya 1986] (see Table 1 for notation):

$$L_o(x,\boldsymbol{\omega_O}) = L_e(x,\boldsymbol{\omega_O}) + \int_{\Omega_+} L_i(x,\boldsymbol{\omega_i}) f(x,\boldsymbol{\omega_i},\boldsymbol{\omega_O})(\boldsymbol{\omega_i}\cdot\mathbf{n}_x)\mathrm{d}\boldsymbol{\omega_i}, \quad (1)$$

where $f(x,\boldsymbol{\omega_i},\boldsymbol{\omega_O})$ is the Bidirectional Reflectance Distribution Function (BRDF) [Nicodemus et al. 1977]. In the rest of the paper, we ignore the notation of the point in the BRDF.

Physically plausible BRDFs obey both *Helmholtz reciprocity* and *energy conservation laws*. Reciprocity means that the incoming and outgoing directions may be exchanged:

$$f(\boldsymbol{\omega_i},\boldsymbol{\omega_O}) = f(\boldsymbol{\omega_O},\boldsymbol{\omega_i}), \quad (2)$$

Energy conservation states that the total reflected power cannot exceed the incident power:

$$\forall\boldsymbol{\omega_O}, \int_{\Omega_+} f(\boldsymbol{\omega_i},\boldsymbol{\omega_O})(\boldsymbol{\omega_i}\cdot\mathbf{n})d\boldsymbol{\omega_i} \leq 1. \quad (3)$$

Parameters of BRDFs can be obtained by fitting to measured data. As real BRDFs are always reciprocal and energy conserving, accurate fitting requires physically plausible BRDF models. In addition, in Monte-Carlo rendering algorithms, BRDF models are best used with their sampling formulas that result in random directions distributed proportionally to the cosine weighted BRDFs.

This paper proposes *physically plausible*, analytical BRDF models with the aim of accurate data fitting, efficient importance sampling and effective real-time rendering. The proposed models are based on halfway vector representation and use the standard *Beckmann* distribution as a *normalized* microfacet distribution. We demonstrate that they can represent both isotropic and anisotropic materials more effectively than existing BRDF models. We also show that Ward's [Ward 1992] importance sampling formulas are good for our proposed BRDF models and are more efficient than Lawrence et al. [Lawrence et al. 2004] factorization method. Furthermore, we demonstrate that our proposed BRDF models are applicable for Monte Carlo rendering algorithms, and material tuning can be done with a few parameters. Finally, we show that our new models not only are well-suited for batch use, but they map well onto modern GPUs with a performance advantage of around 20% over previous methods.

2 Related Work

The first microfacet based BRDF model was proposed by Torrance and Sparrow [Torrance and Sparrow 1967], which was improved by Cook and Torrance [Cook and Torrance 1981]. Although these microfacet based BRDF models are effective in modeling many real materials, they cannot represent anisotropic materials, and do not have efficient importance sampling formulas. Ward's [Ward 1992] and Duer's [Duer 2005] BRDF models are simplifications of the Cook-Torrance model. Their microfacet distribution functions are not *normalized* and are not *physically plausible*. However, they can represent both isotropic and anisotropic materials and have efficient importance sampling formulas.

Neumann et al. [Neumann et al. 1999] analyzed energy conservation of the some analytic models, such as Phong [Phong 1975], Blinn-Phong [Blinn 1977], Cook-Torrance [Cook and Torrance 1981], Ward [Ward 1992] models and they proposed a normalization factor which can be seen as shadowing/masking term to make these models energy conserving. Ashikhmin and Shirley [Ashikhmin and Shirley 2000] proposed an anisotropic variation of the Phong [Phong 1975] reflection model, which was further developed in [Ashikhmin and Premože 2007]. Ashikhmin et al. [Ashikhmin et al. 2000] also introduced a general framework for creating microfacet based BRDF models. We note that the Ashikhmin-Shirley [Ashikhmin and Shirley 2000] microfacet distribution function is not strictly normalized (so this distribution is not physically plausible), since they ignored the $\cos\theta_h$ term when calculating the integral in Equation 7. The correctly *normalized* form of their microfacet distribution function can be found in [Pharr and Humphreys 2004].

Edwards et al. [Edwards et al. 2006] use halfway vector disks for BRDF modeling. Their model is energy conserving and has efficient sampling formulas but it is not *physically plausible* since it is not reciprocal. Lawrence et al. [Lawrence et al. 2004] introduced a new sampling method using nonnegative matrix factorizations (NMF) and demonstrated its effectiveness through comparing to analytical BRDF models such as Lafortune et al. [Lafortune et al. 1997].

Ngan et al. [Ngan et al. 2005] experimentally examined analytical BRDF models. Sun et al. [Sun et al. 2007], Křivánek and Colbert [Krivánek and Colbert 2008] recently demonstrated the possibility of BRDF editing with analytical BRDF models. At the same time, they introduced test beds for analytical BRDF models as well.

*e-mail: murat.kurt@ege.edu.tr
†e-mail: szirmay@iit.bme.hu
‡e-mail: jaroslav@graphics.cornell.edu

Symbol	Meaning
$L_i(x, \omega_i)$	Incident radiance function
$L_o(x, \omega_o)$	Outgoing radiance function
$L_e(x, \omega_o)$	Emitted radiance function
ω_i, ω_o	Unit-lenght incident and outgoing vectors
$\mathbf{n}$	Unit-lenght surface normal vector
$\mathbf{h}$	Unit-lenght halfway vector $(\omega_i + \omega_o)/ \parallel \omega_i + \omega_o \parallel$
Ω_+	Unit hemisphere above the surface
$q(\mathbf{h})$	Non-normalized microfacet distribution function
$D(\mathbf{h})$	Normalized microfacet distribution function
$F(\omega_o \cdot \mathbf{h})$	Fresnel reflectance for incident angle between ω_o and $\mathbf{h}$
$f(\omega_i, \omega_o)$	Bidirectional Reflectance Distribution Function (BRDF)
$p(\omega_i \mid \omega_o)$	Probability density function

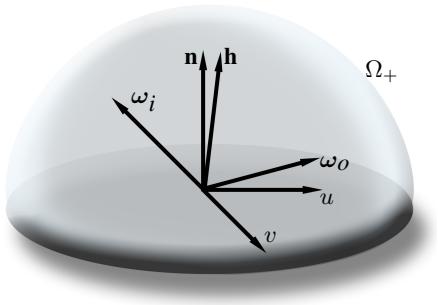

Table 1: *Notation used throughout this paper.*

3 Microfacet Distribution Function

In our analytical anisotropic BRDF model, we use the following *normalized* microfacet distribution function which is *physically plausible*:

$$q(\mathbf{h}) = e^{-\tan^2\theta_h\left(\frac{\cos^2\phi_h}{m_x^2}+\frac{\sin^2\phi_h}{m_y^2}\right)}, \tag{4}$$

$$D(\mathbf{h}) = \frac{1}{\pi m_x m_y \cos^4\theta_h} q(\mathbf{h}). \tag{5}$$

For isotropic materials, $m = m_x = m_y$, thus we get the following microfacet distribution:

$$D(\mathbf{h}) = \frac{1}{\pi m^2 \cos^4\theta_h} e^{-\frac{\tan^2\theta_h}{m^2}}, \tag{6}$$

which is the standard *Beckmann* distribution function [Cook and Torrance 1981].

Our *normalized* microfacet distribution function obeys the following equation

$$\int_0^{2\pi}\int_0^{\pi/2} D(\mathbf{h}) \cos\theta_h \sin\theta_h d\theta_h d\phi_h = 1. \tag{7}$$

This equation means that $D(\mathbf{h})$ is a heighfield distribution, i.e. the total projected area of all the microfacet faces should be equal to the base area [Pharr and Humphreys 2004] ($D(\mathbf{h}) = 0$ if $\cos\theta_h \leq 0$).

4 Energy Conservation and Reciprocity

If a microfacet distribution function is described with *the halfway vector*, then the BRDF model which uses it may satisfy the following equation to fulfill energy conservation [Edwards et al. 2006]:

$$f(\omega_i, \omega_o) \leq \frac{F(\omega_o \cdot \mathbf{h}) D(\mathbf{h})}{4(\omega_o \cdot \mathbf{h})(\omega_i \cdot \mathbf{n})}. \tag{8}$$

Unfortunately, this upper bound does not obey reciprocity. Because of that, as Neumann at al. [Neumann et al. 1999] proposed, we have to make a slight modification:

$$f(\omega_i, \omega_o) = \frac{F(\omega_o \cdot \mathbf{h}) D(\mathbf{h})}{4(\omega_o \cdot \mathbf{h}) \max\{(\omega_i \cdot \mathbf{n}), (\omega_o \cdot \mathbf{n})\}}. \tag{9}$$

This equation produces a *physically plausible* BRDF model if the microfacet distribution function is *normalized*. However, in the course of our experimental analysis on measured BRDF data set, we did not get impressive fitting results with these normalization

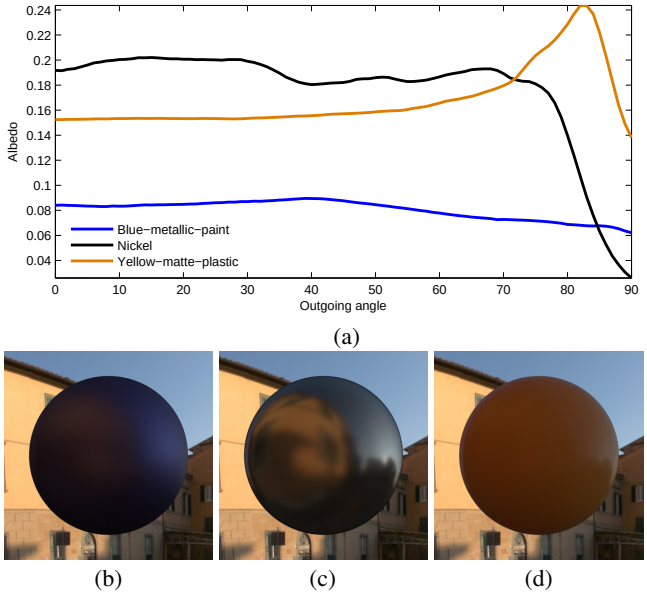

(a)

(b) (c) (d)

Figure 1: *(a) Albedo functions of the measured blue-metallic-paint, nickel and yellow-matte-plastic. (b), (c) and (d) are renderings of these materials.*

factors. Thus, we rather propose to use following BRDF model in data fitting:

$$f(\omega_i, \omega_o) = \frac{F(\omega_o \cdot \mathbf{h}) D(\mathbf{h})}{4(\omega_o \cdot \mathbf{h})((\omega_i \cdot \mathbf{n})(\omega_o \cdot \mathbf{n}))^\alpha}. \tag{10}$$

To show why Equation 10 is better than Equation 9 for data fitting, we first plot the *albedo* functions of measured BRDF data. The *albedo* function depends on outgoing vector ω_o and according to the energy conservation law, its values should not be greater than 1 (Equation 3).

We selected three typical materials from Matusik et al. [Matusik et al. 2003] data set for plotting albedo functions: blue-metallic-paint, nickel, and yellow-matte-plastic. While blue-metallic-paint and nickel are semi-glossy and glossy materials, respectively, yellow-matte-plastic is a specular material and its specularity sharply increases near grazing angles (see Figure 1). Matusik et al. [Matusik et al. 2003] data set contains measurement noise especially at the grazing angles [Edwards et al. 2006; Lawrence et al. 2004]. The plotted albedo functions are also in Figure 1. When the outgoing angle increases, the albedo values of blue-metallic-paint

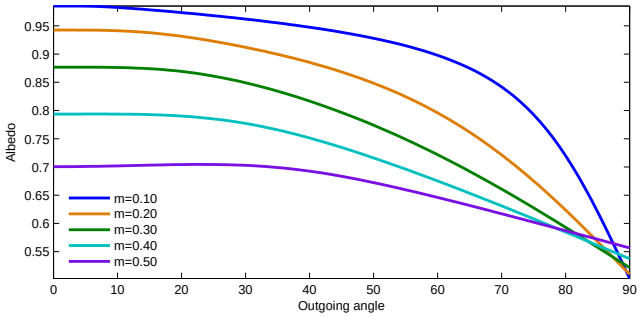

Figure 2: *Albedo functions of the proposed physically-plausible BRDF model (see Equation 9) for different m values. Fresnel term is chosen as* $f_0 = 1.0$.

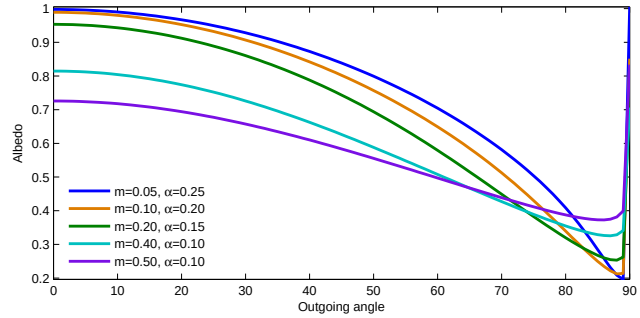

Figure 3: *Albedo functions of the proposed data fitting BRDF model (see Equation 10) for different m and* α *values. If m and* α *are correctly chosen, this model is physically plausible as well. Fresnel term is chosen as* $f_0 = 1.0$.

and nickel decreases, but yellow-matte-plastic behaves differently. Its albedo values increase when the outgoing angle increases and then sharply decreases.

Figure 2 shows the albedo functions of Equation 9 for different m parameters. Note that when the outgoing angle increases, albedo values decrease. With this behavior, diffuse, semi-glossy and glossy materials such as blue-metallic-paint and nickel can be represented well, but this formulation is not suitable for representing specular and highly specular materials such as yellow-matte-plastic. On the other hand, if we plot the albedo functions of Equation 10 for different m and α parameters, we get the plots of Figure 3 that can mimic many kinds of data. If α is set near to 0, diffuse, semi-glossy and glossy materials such as blue-metallic-paint and nickel can be represented well. Furthermore, if α is given a bigger value, specular and highly specular materials such as yellow-matte-plastic can be defined. If α equals to 0, this representation is exactly physically plausible for all m parameters. On the other hand, if α is not equal to 0, the combination of model parameter values determines the physical plausibility (see Figure 3).

5 The New Anisotropic BRDF Model and Its Fitting

A general BRDF model consists of diffuse and specular terms. We develop three different versions of our new anisotropic model. The simple version is the sum of a pure Lambertian term and a single specular lobe:

$$f(\omega_i, \omega_o) = \frac{k_d}{\pi} + \frac{k_s F(\omega_o \cdot \mathbf{h}) D(\mathbf{h})}{4(\omega_o \cdot \mathbf{h})((\omega_i \cdot \mathbf{n})(\omega_o \cdot \mathbf{n}))^{\alpha}} \tag{11}$$

where k_d is the diffuse albedo of the material, k_s is specular reflectivity and $F(\omega_o \cdot \mathbf{h})$ is the Fresnel function of the material, which can be cheaply approximated by Schlick's [Schlick 1994] formula:

$$F(\omega_o \cdot \mathbf{h}) = f_0 + (1 - f_0)(1 - (\omega_o \cdot \mathbf{h}))^5. \tag{12}$$

Based on the observation that the diffuse reflection is due to non-direct photon collisions, the diffuse and specular parts can be *coupled* using the Fresnel function describing ideal mirror reflections:

$$f(\omega_i, \omega_o) = \frac{k_d(1 - F(\omega_o \cdot \mathbf{h}))}{\pi} + \frac{k_s F(\omega_o \cdot \mathbf{h}) D(\mathbf{h})}{4(\omega_o \cdot \mathbf{h})((\omega_i \cdot \mathbf{n})(\omega_o \cdot \mathbf{n}))^{\alpha}}. \tag{13}$$

Finally, we also consider the *multiple-specular lobe* version of the proposed model. Using more than one specular lobe, we can represent the surface roughness on multiple scales, which reduces the fitting error. We also use different Fresnel terms for each specular lobe, which reduces the fitting error as well. In this way, we can model mixture materials like a car paint. The multiple-specular lobe model is:

$$f(\omega_i, \omega_o) = \frac{k_d}{\pi} + \sum_{l=1}^{\#lobes} \frac{k_{sl} F_l(\omega_o \cdot \mathbf{h}) D_l(\mathbf{h})}{4(\omega_o \cdot \mathbf{h})((\omega_i \cdot \mathbf{n})(\omega_o \cdot \mathbf{n}))^{\alpha_l}}. \tag{14}$$

5.1 Fitting the Simple Model

We fitted the proposed simple model to 100 isotropic and 4 anisotropic materials taken from [Matusik et al. 2003], using Ngan's [Ngan et al. 2005] fitting procedure and the L^2 error metric. First, we assumed a single specular lobe.

In our analytical BRDF model, k_d and k_s are the diffuse and specular reflectivities and are linear parameters. On the other hand, f_0, m_x, m_y and α are specular lobe parameters and are non-linear parameters. To produce plausible results, we should include constraints $0 \leq f_0 \leq 1, m_x > 0, m_y > 0$ and $\alpha \geq 0$ in the parameter estimation procedure based on MATLAB FMINCON function.

Brushed aluminum, yellow satin, purple satin and red velvet are four anisotropic materials. Although Ngan et al. [Ngan et al. 2005] underlined that only brushed aluminum and yellow satin are suitable for analytic modeling, we wanted to see the ability of data fitting performance of our analytical BRDF model even for these materials. In Table 2, there are estimated parameters of our model. In Figure 4, renderings of these materials using our anisotropic model can be seen.

We also choose six analytical anisotropic BRDF models for comparing to our model: Ashikhmin-Shirley (A&S) [Ashikhmin and Shirley 2000], Ashikhmin-Premože (A&P) [Ashikhmin and Premože 2007], Edwards et al. [Edwards et al. 2006], Lafortune et al. [Lafortune et al. 1997], Ward [Ward 1992], and Ward-Duer [Duer 2005]. We applied the same fitting procedure to estimate model parameters of these models. Table 3 summarizes the L^2 errors of these models. In Figure 5, we represent brushed aluminum with some of these anisotropic analytical BRDF models. As

Material	k_{dr}	k_{dg}	k_{db}	k_{sr}	k_{sg}	k_{sb}	f_0	m_x	m_y	α	L^2
Brushed alum.	0.0036	0.0034	0.0026	0.0115	0.0105	0.0075	0.999	0.035	0.129	0.005	0.0104
Purple satin	0.0026	0.0004	0.0011	0.1404	0.0522	0.0711	0.055	0.339	1.256	0	0.0006
Red velvet	0.0048	0.0005	0	0.1938	0.0333	0.0267	0.041	2.337	2.644	0	0.0003
Yellow satin	0.0066	0.0022	0.0004	0.0542	0.0345	0.0131	0.207	0.129	1.084	0.197	0.0014

Table 2: *Estimated parameters of our Anisotropic analytical BRDF model on four anisotropic materials which are from Matusik et al. data set.*

Material	A&S	A&P	Edwards	Lafortune	Ward	Ward-Duer	Our Anisotropic
Brushed aluminum	0.0122	0.0106	0.0101	0.0133	0.0104	0.0123	0.0104
Purple satin	0.0006	0.0006	0.0007	0.0008	0.0008	0.0007	0.0006
Red velvet	0.0004	0.0004	0.0004	0.0004	0.0004	0.0004	0.0003
Yellow satin	0.0013	0.0015	0.0017	0.0025	0.0022	0.0020	0.0014

Table 3: *The L^2 errors of seven analytical anisotropic models to four anisotropic data which are from Matusik et al. data set.*

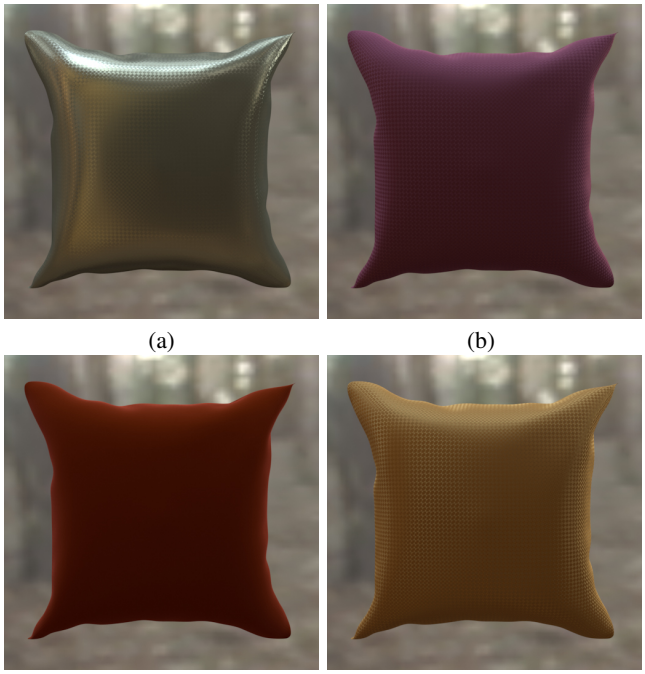

Figure 4: *(a) Brushed aluminum, (b) Purple satin, (c) Red velvet and (d) Yellow satin are reconstructed using our Anisotropic BRDF model. For the model parameters and L^2 errors, see Table 2.*

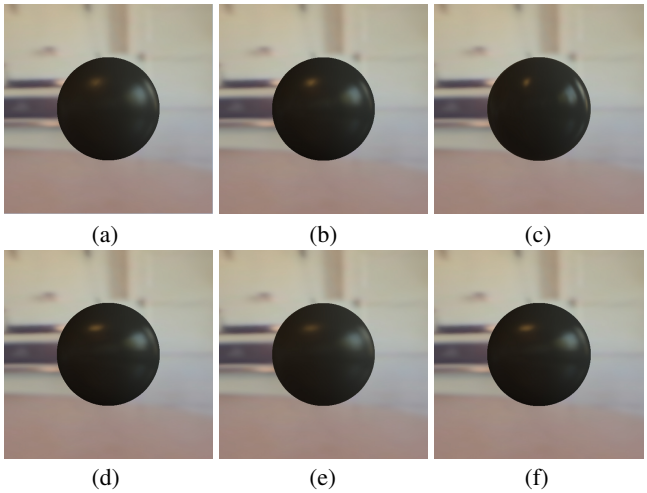

Figure 5: *Brushed aluminum is reconstructed using (a) the Ashikhmin-Shirley, (b) the Ashikhmin-Premože, (c) the Edwards et al., (d) the Ward, (e) the Ward-Duer and (f) our Anisotropic BRDF model. For the model parameters and L^2 errors, see Table 2 and Table 3, respectively.*

it can be seen, our anisotropic BRDF model has better approximation capability than others.

In addition, we choose six analytic isotropic BRDF models for comparing to the isotropic case of our BRDF model: Ashikhmin-Shirley [Ashikhmin and Shirley 2000], Blinn-Phong [Blinn 1977], Cook-Torrance [Cook and Torrance 1981], Lafortune et al. [Lafortune et al. 1997], Ward [Ward 1992] and Ward-Duer [Duer 2005]. We selected 30 materials from Matusik's data set randomly and applied the same fitting procedure to estimate model parameters of these models. In Figure 6, there are the logarithmic L^2 errors of these models. Our BRDF model gives the lowest errors on 25 materials of these 30 materials. Consequently, its approximation capability is effective for isotropic materials as well.

In Figure 7, the polar plots in the incidence plane for four models are shown. Ashikhmin-Shirley [Ashikhmin and Shirley 2000], Cook-Torrance [Cook and Torrance 1981] and Ward [Ward 1992] models have $1/\max\{(\boldsymbol{\omega}_i \cdot \mathbf{n}), (\boldsymbol{\omega}_o \cdot \mathbf{n})\}$,$1/((\boldsymbol{\omega}_i \cdot \mathbf{n})(\boldsymbol{\omega}_o \cdot \mathbf{n}))$ and $1/\sqrt{(\boldsymbol{\omega}_i \cdot \mathbf{n}), (\boldsymbol{\omega}_o \cdot \mathbf{n})}$ terms, respectively, and they act as shadowing/masking terms. However, they are not optimized for one material and do not vary from material to material. Our proposed anisotropic BRDF model optimizes this shadowing/masking term with an additional α parameter. In this way, it more closely matches the measured BRDF data than existing BRDF models.

5.2 Multiple Specular Lobes

We choose six analytical BRDF models: Ashikhmin-Shirley [Ashikhmin and Shirley 2000], Blinn-Phong [Blinn 1977], Cook-Torrance [Cook and Torrance 1981], Ward [Ward 1992], Ward-Duer [Duer 2005] and our proposed model. We fitted them to randomly selected 30 materials form Matusik's data set, and used the two specular lobe versions of each model. In Figure 8, there are the logarithmic L^2 errors of these models. Our BRDF model gives the lowest errors on 28 materials out of 30 materials. Although the addition of specular lobes decreases

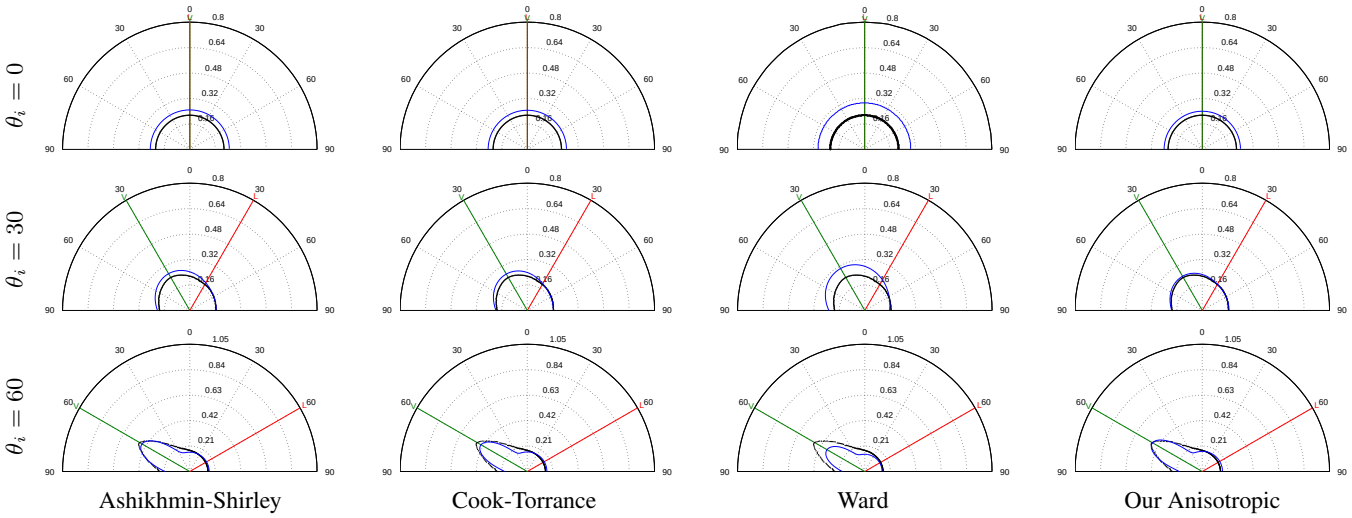

Figure 7: *Polar plots of various fitted models against the measured BRDF (black dashed lines) of "dark-specular-fabric" in the incidence plane. Cubic root applied for visualization purpose. The Ashikhmin-Shirley L^2 error is 0.0042, the Cook-Torrance L^2 error is 0.0036, the Ward L^2 error is 0.0132 and our Anisotropic model L^2 error is 0.0027 for this material.*

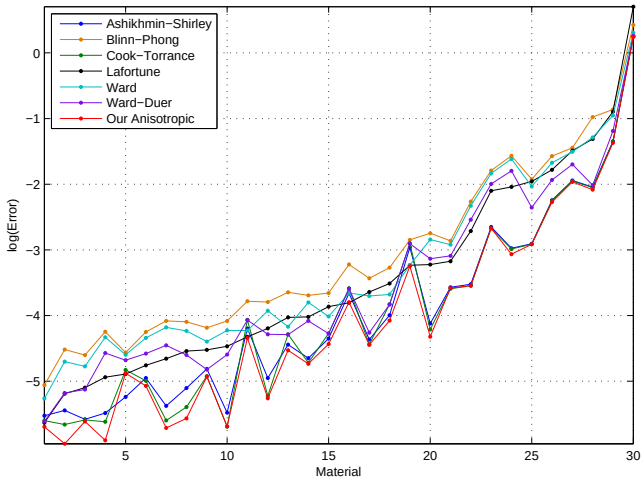

Figure 6: *L^2 errors (logarithmic scale) of seven analytic models to 30 isotropic BRDF data which are from Matusik et al. data set. The BRDFs are sorted in the errors of the Lafortune model (Black) for visualization purpose. One specular lobe is used for all models.*

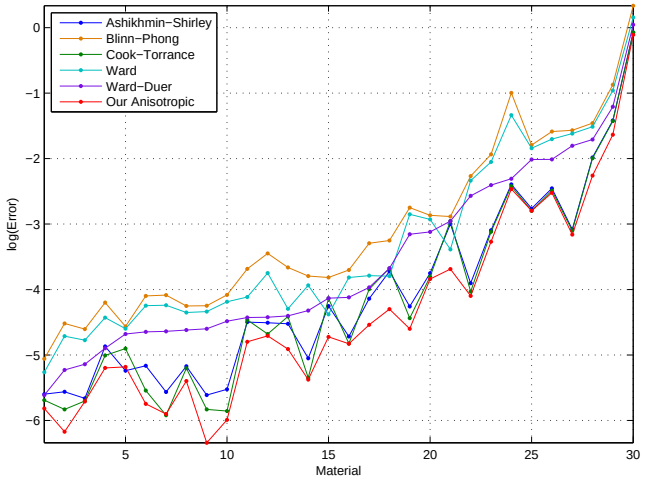

Figure 8: *L^2 errors (logarithmic scale) of six analytic models to 30 isotropic BRDF data which are from Matusik et al. data set. The BRDFs are sorted in the errors of the Ward-Duer model (Magenta) for visualization purpose. Two specular lobes are used for all models.*

the errors and increases the visual quality, its effectiveness varies from model to model. In these 30 materials, one extra specular lobe reduces the error by 4.00% in the Blinn-Phong model, 7.00% in the Ward model, 11.41% in the Ward-Duer model, 20.72% in the Ashikhmin-Shirley model, 21.42% in the Cook-Torrance model and by 27.62% in our proposed model. Consequently, its approximation capability is even more effective when it is used with multiple lobes.

Moreover, we choose six BRDF representations for visually comparing to the isotropic case of our BRDF model: Ashikhmin-Shirley [Ashikhmin and Shirley 2000], Cook-Torrance [Cook and Torrance 1981], Edwards et al. [Edwards et al. 2006], Lawrence et al. [Lawrence et al. 2004], Ward [Ward 1992] and Ward-Duer [Duer 2005]. We selected three materials (blue-metallic-paint, nickel and yellow-matte-plastic) from Matusik's data set and applied the same fitting procedure to estimate model parameters of the analytical models. To increase fitting quality, we used three specular lobes for the analytical models. We used the same scene configuration for rendering as Edwards et al. [Edwards et al. 2006] used in their work. Figure 9 shows renderings of the Princeton scene [Edwards et al. 2006]. The table was rendered with the approximation of measured nickel in this scene. Since the viewer looks at the table from grazing angles, it is distinctive for approximation capability. We also calculated the PSNR (Peak Signal-to-Noise Ratio) values for each color channel and obtained their averages [Richardson 2002]. The PSNR values and difference images between the reference image and rendered images are also presented in Figure 9. Results indicate that our proposed BRDF model most closely matches the measured BRDF data. Furthermore, while our proposed BRDF model requires only few parameters to represent materials, Lawrence et

(a) Reference image
(b) Ashikhmin-Shirley (PSNR=31.8419)
(c) Cook-Torrance (PSNR=31.1835)
(d) Edwards (PSNR=26.4502)

(e) Lawrence (PSNR=30.3722)
(f) Ward (PSNR=22.2599)
(g) Ward-Duer (PSNR=31.7116)
(h) Our Anisotropic (PSNR=32.1210)

Figure 9: *Visual comparisons of well-known BRDF representations on the Princeton scene. (a) Reference image was rendered using measured BRDF data. (b), (c), (d), (e), (f), (g), (h) were rendered using the Ashikhmin-Shirley, the Cook-Torrance, the Edwards et al., the Lawrence et al. factored BRDF, the Ward, the Ward-Duer and our Anisotropic BRDF model, respectively. While (a), (b), (c), (d), (f), (g) and (h) were rendered at 262144 samples/pixel, (e) was rendered at 4096 samples/pixel. Insets show a difference between the reference image and the rendered image and darker portions in these difference images mean higher disparity. Below each image we also report (PSNR value).*

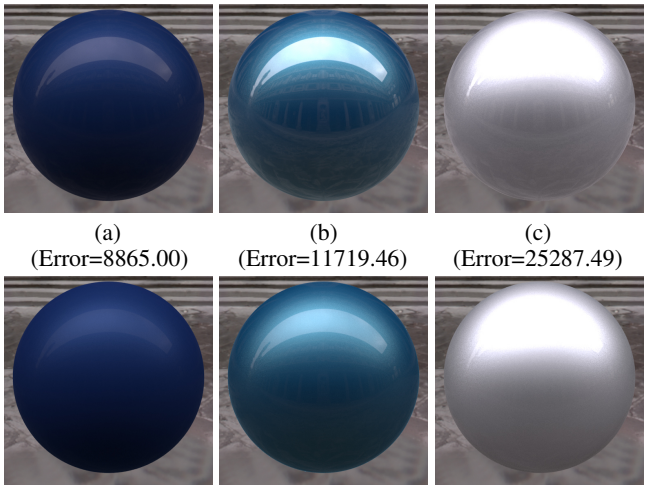

(a) (Error=8865.00)
(b) (Error=11719.46)
(c) (Error=25287.49)
(c) (Error=8051.00)
(d) (Error=10302.48)
(e) (Error=24950.82)

Figure 10: *(a) Specular blue, (b) Green-blue flip-flop, (c) Silver metallic are reconstructed using the Cook-Torrance BRDF model. (d) Specular blue, (e) Green-blue flip-flop, (f) Silver metallic are reconstructed using our Anisotropic BRDF model. Below each image we also report (Error value).*

al. [Lawrence et al. 2004] required 176KB, 120KB and 384KB for representing blue-metallic-paint, nickel and yellow-matte-plastic, respectively.

Furthermore, we fitted isotropic case of our model to another BRDF data set which was measured by Rump et al. [Rump et al. 2008]. This data set includes three metallic car paints: specular blue, green-blue flip-flop and silver metallic. When we fitted analytical models to this data set, we used Rump et al.'s [Rump et al. 2008] fitting procedure and error metric. As can be seen from Figure 10, our model represents metallic car paints better than the Cook-Torrance BRDF model.

6 Importance Sampling

In Monte Carlo rendering algorithms the outgoing radiance is obtained as:

$$L_o(\omega_o) \approx \frac{1}{\#samples} \sum_{i=1}^{\#samples} L_i(\omega_i) \frac{f(\omega_i, \omega_o)(\omega_i \cdot \mathbf{n})}{p(\omega_i \mid \omega_o)}. \tag{15}$$

In above equation, probability density function $p(\omega_i \mid \omega_o)$ should mimic $f(\omega_i, \omega_o)(\omega_i \cdot \mathbf{n})$ for efficient importance sampling.

Let ξ_1 and ξ_2 be two canonical uniform random variables in the range $0 \leq \xi_1 < 1, 0 \leq \xi_2 < 1$. Importance sampling equations for

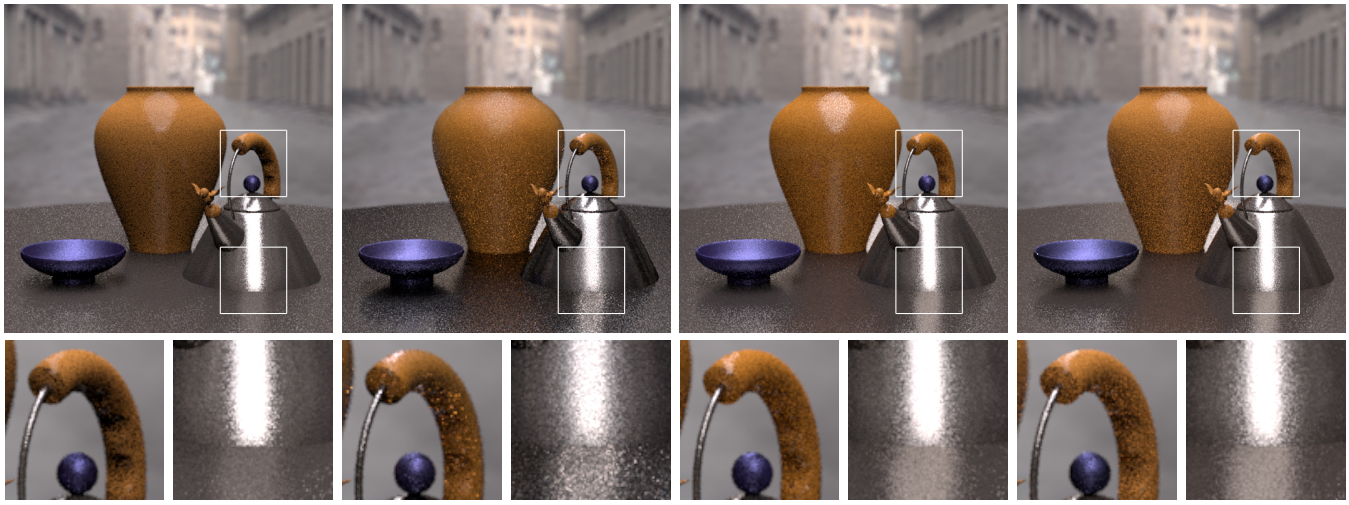

(a) Edwards sampling 64 samples/pixel | (b) Lawrence sampling 64 samples/pixel | (c) Ward-Duer sampling 64 samples/pixel | (d) Our Anisotropic sampling 64 samples/pixel

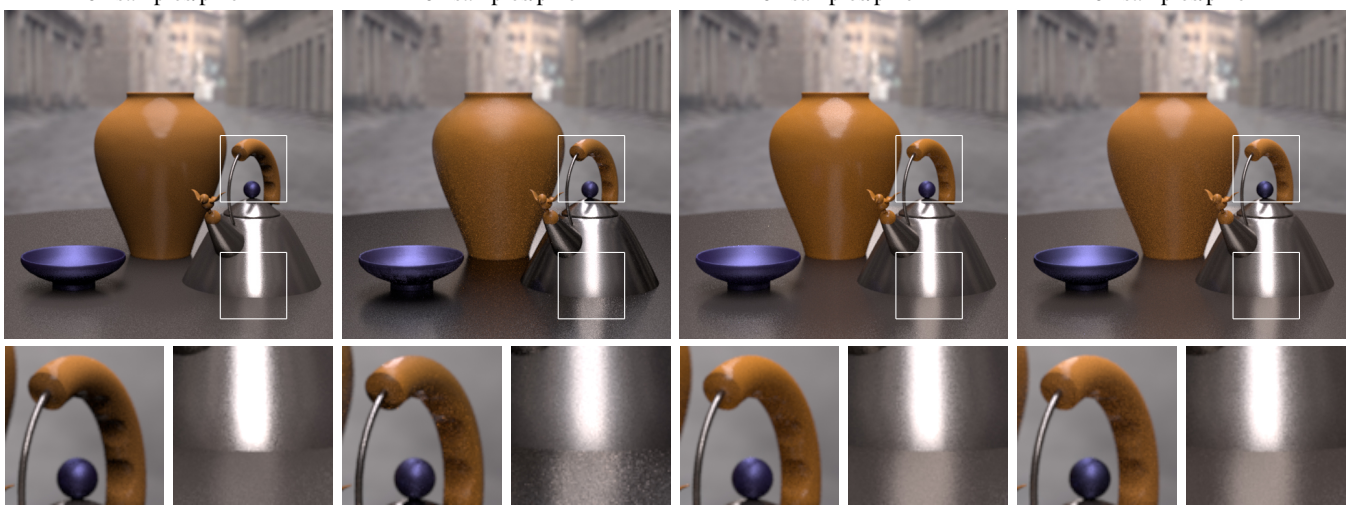

(e) Edwards sampling 4096 samples/pixel | (f) Lawrence sampling 4096 samples/pixel | (g) Ward-Duer sampling 4096 samples/pixel | (h) Our Anisotropic sampling 4096 samples/pixel

Figure 11: *The Princeton scene with global illumination was rendered using a path tracing algorithm for visual comparison of sampling efficiency. Paths up to five bounces long were included. While (a), (b), (c) and (d) were rendered using the Edwards et al., the Lawrence et al., the Ward-Duer and our Anisotropic model at 64 samples/pixel, respectively, (e), (f), (g) and (h) were rendered using the Edwards et al., the Lawrence et al., the Ward-Duer and our Anisotropic model at 4096 samples/pixel, respectively. The bottom rows show closeups of the highlighted regions.*

our anisotropic BRDF model are:

$$\theta_h = \arctan\left(\sqrt{\frac{-\log(\xi_1)}{\frac{\cos^2\phi_h}{m_x^2}+\frac{\sin^2\phi_h}{m_y^2}}}\right), \tag{16}$$

$$\phi_h = \arctan\left(\frac{m_y}{m_x}\tan(2\pi\xi_2)\right). \tag{17}$$

With the help of Equation 16 and Equation 17, we can calculate the *halfway vector* $\mathbf{h}$:

$$\mathbf{h} = [\sin\theta_h\cos\phi_h, \sin\theta_h\sin\phi_h, \cos\theta_h]. \tag{18}$$

After that, we can find the sampling direction $\boldsymbol{\omega}_i$ with the following formula:

$$\boldsymbol{\omega}_i = 2(\boldsymbol{\omega}_o\cdot\mathbf{h})\mathbf{h} - \boldsymbol{\omega}_o. \tag{19}$$

Probability density function $p(\boldsymbol{\omega}_i \mid \boldsymbol{\omega}_o)$ for our anisotropic BRDF model is:

$$p(\boldsymbol{\omega}_i \mid \boldsymbol{\omega}_o) = \frac{1}{4\pi m_x m_y \cos^3\theta_h(\boldsymbol{\omega}_o\cdot\mathbf{h})}q(\mathbf{h}), \tag{20}$$

where $q(\mathbf{h})$ is from Equation 4. For the derivation of sampling formulas, see Walter's [Walter 2005] notes.

The ratio of the product of the BRDF and cosine of the orientation angle and the sampling density (see Equation 15) will be the weight of the sample. For our anisotropic BRDF model, weighting function is the following:

$$w(\boldsymbol{\omega}_i \mid \boldsymbol{\omega}_o) = \frac{k_s F(\boldsymbol{\omega}_o\cdot\mathbf{h})(\boldsymbol{\omega}_i\cdot\mathbf{n})^{1-\alpha}}{\cos\theta_h(\boldsymbol{\omega}_o\cdot\mathbf{n})^{\alpha}}. \tag{21}$$

Actually, the sampling procedure of the our anisotropic model is the same as that of the Ward's [Ward 1992] model. However, our

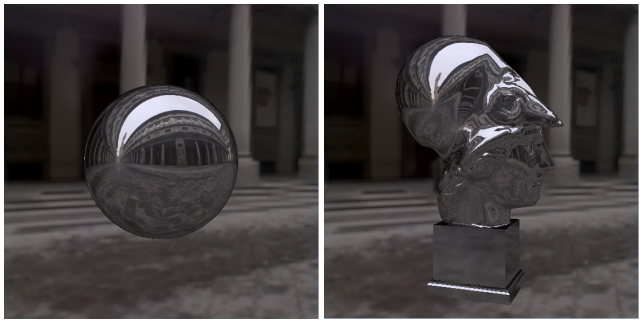

(a) Sphere (b) Athena

Figure 12: *Various objects rendered with isotropic version of our analytic BRDF model. For all scenes,* $m = m_x = m_y = 0.001, f_0 = 0.5, \alpha = 0.25, k_d = [0, 0, 0], k_s = [1.0, 1.0, 1.0]$.

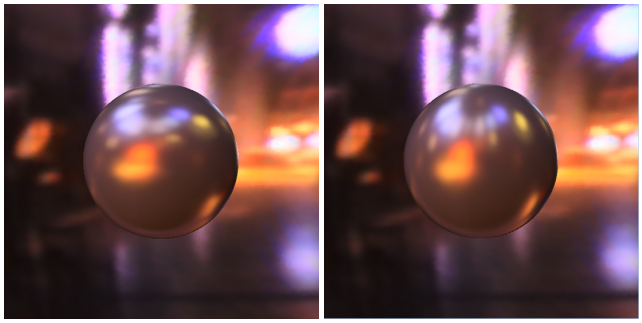

(a) $m_x = 0.05, m_y = 0.1$ (b) $m_x = 0.1, m_y = 0.05$

Figure 13: *A sphere rendered with anisotropic version of our analytic BRDF model. For both scenes,* $k_d = [0.15, 0.15, 0.15]$, $k_s = [0.85, 0.85, 0.85]$, $f_0 = 0.75$ *and* $\alpha = 0.2$.

weighting function is different, which makes our model have different importance sampling efficiency. If our model did not contain the Fresnel term, the importance sampling efficiency would be better than that of Ward's [Ward 1992] BRDF model.

Furthermore, we compared sampling efficiency of our anisotropic model to Edwards et al. [Edwards et al. 2006] sampling method, Lawrence et al. [Lawrence et al. 2004] factorization method, and Ward-Duer [Duer 2005] sampling method. We used the same scene configuration as in Figure 9. Visual comparison of sampling quality is shown in Figure 11. Figure 11 also includes closeup views of some important regions, such as the teapot handle. As Figure 11 demonstrates, we obtain better sampling efficiency than Lawrence et al. [Lawrence et al. 2004] factored representation. As a consequence of this, our anisotropic BRDF model can be used both for representing and importance sampling the BRDFs.

7 Real-Time Rendering Implementation

We tested and compared our anisotropic analytical model in a GPU-based real-time rendering algorithm [Kriv\u00e1nek and Colbert 2008]. In real-time rendering implementation, we used Fresnel blended version of the our BRDF model (see Equation 13). As we mentioned before, when $m_x = m_y$, our BRDF model is used to represent isotropic materials (see Equation 6). In Figures 12 and 13, the isotropic and anisotropic cases of our BRDF model can be seen, respectively.

Moreover, the rendering frame rates for varying environment maps are shown in Figure 14. Although Figure 14 does not contain FPS

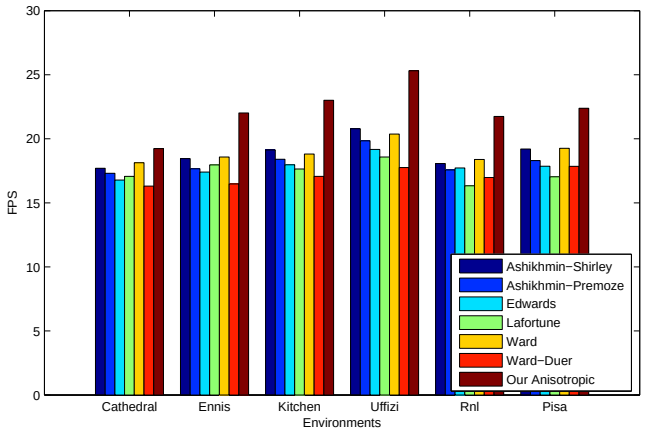

Figure 14: *Plot of the real-time rendering performance with respect to the number of frame per second (FPS) for a given environments when rendering a sphere at a resolution of* 550×550. *The 40 samples were used during rendering.*

Figure 15: *Material design can be done with analytical BRDF models on the fly. This is true for our proposed Anisotropic model as well.*

values for the Blinn-Phong model, we found average of 34.575 FPS for it. As can be seen from Figure 14, our anisotropic BRDF model has effective real-time rendering performance. These results were produced on a consumer-level PC with Intel Pentium 4 3.00GHz processor, 2GB RAM and a Nvidia GeForce 6600 GT 256MB graphics card.

Finally, material design can be done with our anisotropic model interactively (see Figure 15).

8 Conclusions and Future Work

In this work, we have provided a comprehensive review of analytical BRDF models and proposed new physically plausible

anisotropic BRDF models. Our proposed models are based on halfway vectors, have *normalized* microfacet distribution function, have efficient importance sampling procedure and efficient performance in both data fitting and real-time rendering. We also tested them in a real-time rendering algorithm and have shown that material editing can be done dynamically.

As a future work, we would like to use our *physically plausible* models in Bidirectional Scattering Distribution Function (BSDF) which equals to sum of BRDF and Bidirectional Transmittance Distribution Function (BTDF).

References

ASHIKHMIN, M., AND PREMOŽE, S., 2007. Distribution-based BRDFs. Unpublished technical manuscript.

ASHIKHMIN, M., AND SHIRLEY, P. 2000. An anisotropic Phong BRDF model. *Journal of Graphics Tools 5*, 2, 25–32.

ASHIKHMIN, M., PREMOŽE, S., AND SHIRLEY, P. 2000. A microfacet-based BRDF generator. In *Proceedings of SIGGRAPH 2000*, 65–74.

BLINN, J. F. 1977. Models of light reflection for computer synthesized pictures. In *Proceedings of SIGGRAPH 77*, 192–198.

COOK, R. L., AND TORRANCE, K. E. 1981. A reflectance model for computer graphics. In *Proceedings of SIGGRAPH 81*, 307–316.

DUER, A., 2005. On the Ward model for global illumination. Unpublished material.

EDWARDS, D., BOULOS, S., JOHNSON, J., SHIRLEY, P., ASHIKHMIN, M., STARK, M., AND WYMAN, C. 2006. The halfway vector disk for BRDF modeling. *ACM Trans. Gr. 25*, 1 (January), 1–18.

KAJIYA, J. T. 1986. The rendering equation. In *Proceedings of SIGGRAPH 86*, 143–150.

KRIVÁNEK, J., AND COLBERT, M. 2008. Real-time shading with filtered importance sampling. *Computer Graphics Forum 27*, 4, 1147–1154.

LAFORTUNE, E. P., FOO, S.-C., TORRANCE, K. E., AND GREENBERG, D. P. 1997. Non-linear approximation of reflectance functions. In *Proceedings of SIGGRAPH 97*, 117–126.

LAWRENCE, J., RUSINKIEWICZ, S., AND RAMAMOORTHI, R. 2004. Efficient BRDF importance sampling using a factored representation. *ACM Trans. Graph. (Proceedings of SIGGRAPH 2004) 23*, 3, 496–505.

MATUSIK, W., PFISTER, H., BRAND, M., AND MCMILLAN, L. 2003. A data-driven reflectance model. *ACM Trans. Gr. 22*, 3 (July), 759–769.

NEUMANN, L., NEUMANN, A., AND SZIRMAY-KALOS, L. 1999. Compact metallic reflectance models. *Computer Graphics Forum 18*, 3 (September), 161–172.

NGAN, A., DURAND, F., AND MATUSIK, W. 2005. Experimental analysis of BRDF models. In *Proc. of the Eurographics Symposium on Rendering*, 117–226.

NICODEMUS, F. E., RICHMOND, J. C., HSIA, J. J., GINSBERG, I. W., AND LIMPERIS, T. 1977. Geometrical considerations and nomenclature for reflectance. Monograph, National Bureau of Standards (US), October.

PHARR, M., AND HUMPHREYS, G. 2004. *Physically Based Rendering: From Theory to Implementation*. Morgan Kaufmann Publishers Inc., San Francisco, CA, USA.

PHONG, B. T. 1975. Illumination for computer generated pictures. *Commun. ACM 18*, 6 (June), 311–317.

RICHARDSON, I. E. 2002. *Video Codec Design: Developing Image and Video Compression Systems*. John Wiley & Sons, Inc., New York, NY, USA.

RUMP, M., MÜLLER, G., SARLETTE, R., KOCH, D., AND KLEIN, R. 2008. Photo-realistic rendering of metallic car paint from image-based measurements. *Computer Graphics Forum 27*, 2 (April), 527–536.

SCHLICK, C. 1994. An inexpensive BRDF model for physically-based rendering. *Computer Graphics Forum 13*, 3, 233–246.

SUN, X., ZHOU, K., CHEN, Y., LIN, S., SHI, J., AND GUO, B. 2007. Interactive relighting with dynamic BRDFs. *ACM Trans. Graph. (Proceedings of SIGGRAPH 2007) 26*, 3, 27.

TORRANCE, K. E., AND SPARROW, E. M. 1967. Theory for off-specular reflection from roughened surfaces. *Journal of the Optical Society of America 57*, 9 (September), 1105–1114.

WALTER, B. 2005. Notes on the ward BRDF. Technical report PCG-05-06, Program of Computer Graphics, Cornell University, April.

WARD, G. J. 1992. Measuring and modeling anisotropic reflection. In *Proceedings of SIGGRAPH 92*, 265–272.